Disposed Material Mobility and Transport in the Vicinity of the Charleston Ocean Dredged Material Disposal Site

George Voulgaris
Coastal Processes and Sediment Dynamics Laboratory
Marine Science Program – Department of Geological Sciences
University of South Carolina
Columbia, SC 29208

Final Report Submitted to the
SC Department of Natural Resources
Marine Resources Division
P.O. Box 12559
217 Ft. Johnson Road
Charleston, SC 29422

Technical Report: CPSD/02/01

June 2002

Executive Summary

A experimental field study was carried out during the period July 6th – August 20th, 2001; it aimed at providing data and some insight on sediment mobility in the vicinity of the permitted disposal zone within the Charleston ODMDS. The study focused primarily on the deployment of a bottom boundary layer tripod for the monitoring of bottom turbulence due to the combined action of waves and currents and sediment remobilization and transport. Additional data included measurements of water density and spatial variability of flow along the western berm for a period of two tidal cycles.

Due to biofouling, the optical sensors ceased operating within eight to ten days after the day of deployment. A one-dimensional sediment resuspension and transport model was verified using the first eight days of sediment transport, and then used for predicting sediment transport for the remainder of the deployment period when no sediment data were collected.

The major findings of this study were:

- Wind-driven circulation is the most important factor in controlling sediment transport. Strong winds generate waves that steer the sediment on the seabed and create large nearbed suspended sediment concentrations. The winds also drive wind-driven flows that transport the resuspended sediment along the direction of the mean current.

- High correlation of wind data from Folly Island and near bed flows suggests that the meteorological data can be used as a first order approximation of transport pathways (near bed).

- Suspended sediment transport is directed mainly NE and SW in response to local wind climate and the wind-generated alongshore flows. During the measurement period, the NE transport dominated the signal. This transport direction appears to be parallel to the direction of the main western berm thus questioning the effectiveness of this berm in trapping sediment. The observed sediment transport direction is typical for the area. However, analysis of 8 years of wind data revealed that more sediment transport towards SW should occur in response to NE winds, which were very weak during the study period.

- Given the NE-SW sediment transport direction, the construction of the northeastern (bathymetric high in Figure 3) and southwestern berms might be more effective in confining some of the disposed sediment.

- Fine particles appear to be in suspension for the majority of the time, and in particular following a resuspension event. The low settling velocities in conjunction with the wave activity in breaking up flocculate material (Hill et al., 2001) allow the fine particles to remain in resuspension for long periods (over 24 hours) and dispersed in the area.

Finally, we recommend monitoring of the particle size distribution of the suspended sediment as well as the concentration at a minimum of three locations: SE of the site, inside the site and NE of the site. This approach will reveal the transport of fines (single particles or flocculates) and the effectiveness of the berms in trapping sediment. Further, it will help develop priorities in berm construction dumping management. A 2-D circulation and sediment transport model that incorporates the effects of advection in sediment transport pathways and the wind field in the ODMDS site should accompany the monitoring efforts.

List of Contents

LIST OF CONTENTS ..... **III**

LIST OF TABLES ..... **VI**

1. INTRODUCTION **1**

2. MEASUREMENTS **2**

2.1 BENTHIC BOUNDARY LAYER MEASUREMENTS 3
2.2 MAPPING OF TIDAL CURRENTS OVER THE ODMDS FOR A FULL TIDAL CYCLE. 4
2.3 AUXILIARY DATA 5

3. DATA ANALYSIS & RESULTS **5**

3.1 AVERAGED TIME-SERIES. 5
3.2 TIDAL ANALYSIS AND WIND-DRIVEN FLOWS. 7
3.3 WAVE CHARACTERISTICS. 11
3.4 BOTTOM STRESS ESTIMATES 12
3.5 MODELING OF HYDRODYNAMICS AND SUSPENDED SEDIMENT TRANSPORT. 14
3.6 MAPPING OF THE MEAN CURRENT FIELD AROUND THE BERM. 23

4. CONCLUSIONS **23**

5. RECOMMENDATIONS **24**

ACKNOWLEDGEMENTS **24**

LIST OF REFERENCES **25**

APPENDICES **26**

List of Figures

Figure 1. Diagram showing the location of the study area in relation to the coastline. The NOAA NDBC meteorological-station at Folly Beach and Charleston Harbor tidal station (NOAA NOS) locations are shown. The cross to the west of the southern end of the western berm indicates the location of the benthic boundary layer measurements (tripod). The outline of the ODMDS area is shown in red, while the dashed square indicates the boundaries of the study area shown in more detail in Figure 3. The small red square at the east corner of the ODMDS site is the location of the current measurements described by Williams et al. (1987). Bathymetry data shown here was collected by the US Geological Survey and Center for Marine and Wetland Studies in March 2000 (Gayes 2000). **2**

Figure 2. Photograph showing the Coastal Processes & Sediment Dynamics (CPSD) Laboratory tripod used for the data collection. **3**

Figure 3. Detailed bathymetric map of the ODMDS (data from Gayes 2000) showing the western berm (shallow, hot colors) and the location of the tripod deployment (green circle). ADCP survey lines and locations of the CTD stations (red circles) in the NE and SW ends of the berm are also shown. The outline of the ODMDS is shown as a red, dashed line. **4**

Figure 4. Time-series of burst-averaged values of local water depth (top panel), east and north components of flow (middle panel) and OBS-measured turbidity levels. Notice the turbidity level background increasing after day 195 (deployment day 8) due to biofouling. **6**

Figure 5. Time-series of: (a) east and north components of wind velocity (oceanographic convention) and (b) total wind speed for the period of the experimental data collection. **7**

Figure 6 Near bed tidal current ellipses of the most important tidal constituents. **8**

Figure 7. Results of harmonic analysis of sea surface elevation: (a) predicted tide (blue); (b) residual sea surface elevation due to wind forcing (red). **8**

Figure 8. Results of harmonic analysis of the north component of the nearbed currents. Top: raw time-series. Bottom: predicted tides (blue) and residual wind-driven current (red). **9**

Figure 9. Results of harmonic analysis of the east component of the nearbed currents. Top: raw time-series. Bottom: predicted tides (blue) and residual wind-driven current (red). **9**

Figure 10 Progressive and resultant vectors for tidal (blue), wind-induced (red) and for combined tidal and wind-induced circulation (black) over the 28.9 -day period of data collection. The similarity in magnitude and direction of the resultant vectors for the case of wind only (red dashed line) and wind and tidal circulation (black dashed line) clearly demonstrate the importance of the wind driven circulation in **10**

transporting water masses in the study area.

Figure 11. Time-series of wave characteristics as calculated from the spectral analysis of the pressure and velocity records. **11**

Figure 12 Polar diagram showing the wave-climate for the period of the measurements. Dashed line indicates the general orientation of the coastline. The majority of the waves are mild with periods between 6 and 10 sec and a direction of approach from the ESE. Bigger waves (red crosses) occur during wind activity, are locally generated, have a wave period of approximately 5 to 7 sec and a direction from the south or the NE. **12**

Figure 13. Comparison of mean current shear velocities estimated using the inertial dissipation (ID) method and the Reynolds stress technique. The 1:1 line is also shown for reference. **13**

Figure 14 Estimation of bottom drag coefficient, Cd, from the Reynolds Stress derived mean shear stress. **14**

Figure 15. Particle size analysis results for bed sediment samples collected from the tripod deployment site (right) and the western berm location (left). Notice the slightly higher percentage of fines found over the berm. (Note: particle size units are in Phi where Phi=-$\log_2$(d in mm)). **15**

Figure 16. Model prediction of mean current shear velocity (blue) and maximum combined wave and current shear velocity (red). Notice the contribution of the waves significantly increases the bottom shear velocity and thus contributes more to sediment mobility **16**

Figure 17. A comparison of the measured mean shear velocity to shear velocity as predicted by the model. The model appears to slightly under-predict shear velocities at high-energy conditions and to over-predict at low energy conditions. However, the overall agreement is satisfactory for the purposes of establishing sediment transport pathways **17**

Figure 18. (a) Measured turbidity in the field using the OBS. Counts are linearly related to the amount of sediment in suspension in the water column. (b) Suspended sediment concentration as predicted by the model for the period of OBS measurements. Four major resuspension events are captured by the model (see days 188-190, 192-194, 195-196 and 198-200). The same events can be seen on the measurements but they are less distinct. The blurring of the events shown in the measurements is due to advection and to fine material being in suspension for a long time. The arrows on (b) are indicative of how advection of fine material from a resuspension event will be advected to elevate suspended sediment concentration levels at other times as indicated by the measurements. **17**

Figure 19. Left Panel: Local suspended sediment flux as measured at 40cm above the bed during the period of the deployment using data not affected by bio-fouling. Right Panel: Depth-integrated suspended sediment flux as predicted by the model assuming no-cohesive material and for the same period as in the left panel. (Note: count is the recorded output of the OBS sensor and it is a linear proxy of suspended **18**

sediment concentration).

Figure 20. Depth-integrated local suspended sediment transport vectors predicted by the 1-D model under the combined action of waves and currents for the whole period of data collection. The sediment is transported into major directions NE and SW while minimal transport is predicted toward the shore or away from it. **19**

Figure 21. Cumulative sediment transport over the period of data collection **20**

Figure 22. Rose-diagrams of wind direction (oceanographic convention) from the NOAA NBDC Folly beach meteorological station, for four different groups of wind intensity. The data analyzed to produce these diagrams were hourly wind speeds and directions covering the period 1984 to 2001. The numbers shown on the co-centric grids are number of occurrences **22**

Figure 23. Rose-diagram of wind direction (oceanographic convention) and histogram of wind speed, from the NOAA NBDC Folly beach meteorological station, for the 28.9-day period of this study **23**

List of Tables

Table 1. List of the particle size fractions and their corresponding frequency of occurrence as used in the sediment resuspension and transport model. **15**

1. INTRODUCTION

The Charleston, South Carolina Ocean Dredge Material Disposal Site (ODMDS) is one of the most active, frequently used disposal sites in the South Atlantic Bight. Dredging and disposal of dredged material is often associated with potential environmental impacts that require continuous monitoring.

The design and initial planning of the ODMDS were based on ocean current data collected by the U.S Environmental Protection Agency (EPA) in summer and winter 1991 and the National Oceanic and Atmospheric Administration (NOAA), National Ocean Services (NOS) in conjunction with a circulation survey of the Charleston Harbor (Wilmot 1988). These data showed that during most of the year a NNE flow prevails, while during the winter there is an additional western component of flow in response to northeastern winds.

NOAA (Williams *et al*. 1987) carried out additional long-term current measurements covering the period 01/20/1994 to 09/28/1995. Analysis of the currents revealed that the major tidal component is the M_2 (principal lunar semi-diurnal constituent) with amplitude of approximately 20cm/s and major ellipse orientation perpendicular to the coastline. Wind-driven flows were found to be towards the NE or SW in a direction parallel to the coastline. This study concluded that wind-driven flow is responsible for transporting the pollutants in this area. However, no direct measurements on sediment mobility or wave activity were carried out.

The overall objective of the present study is to provide data on sediment mobility in the benthic boundary layer in the vicinity of the permitted disposal zone within the Charleston ODMDS (referred to here as the ODMDS: (NAD83), 32.65663^o N, 79.75716^o W; 32.64257^o N, 79.72733^o W; 32.61733^o N, 79.74381^o W; and 32.63142^o N, 79.77367^o W) under the combined action of waves and currents.

Following the approval of the US Army Corps of Engineers, SC DNR placed a work order to the Department of Geological Sciences, University of South Carolina for the following tasks:

1) Measurements of the combined action of the waves and currents in the disposal site.
2) Measurements of the local suspended sediment concentration.
3) Mapping of the mean current field around the berm.
4) Calculations of threshold conditions for the re-suspension of sediment.
5) Estimations of sediment transport magnitude and direction.

This report describes the data collection and analysis that was carried out as part of this work order.

2. MEASUREMENTS

The measurement program took place within the vicinity of the western containment berm of the ODMDS and consisted of:

(i) Deployment of a benthic boundary layer tripod for the measurement of near bed turbulence and sediment dynamics; and
(ii) Mapping of tidal currents over the western ODMDS berm for two tidal cycles.

Additional data used in this study included tidal gauge and meteorological data. The location of the ODMDS study area in relation to the coastline is shown in Figure 1.

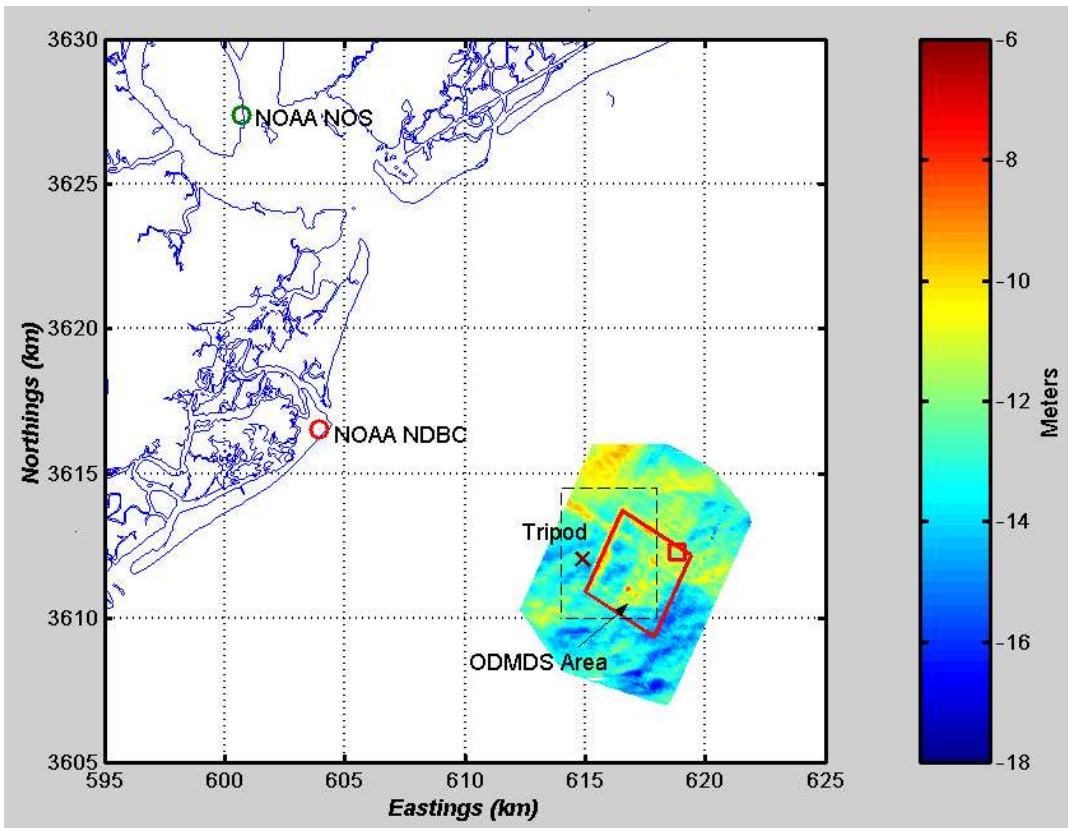

Figure 1. Diagram showing the location of the study area in relation to the coastline. The NOAA NDBC meteorological-station at Folly Beach and Charleston Harbor tidal station (NOAA NOS) locations are shown. The cross to the west of the southern end of the western berm indicates the location of the benthic boundary layer measurements (tripod). The outline of the ODMDS area is shown in red, while the dashed square indicates the boundaries of the study area shown in more detail in Figure 3. The small red square at the east corner of the ODMDS site is the location of the current measurements described by Williams et al. (1987). Bathymetry data shown here was collected by the US Geological Survey and Center for Marine and Wetland Studies in March 2000 (Gayes 2000).

2.1 Benthic Boundary Layer Measurements

Bottom boundary layer measurements were obtained by deploying an instrumented tripod (Figure 2) developed at the Coastal Processes and Sediment Dynamics (CPSD) Laboratory of the University of South Carolina. The tripod was deployed on July 6th, 2001 (Julian Day 2001:187) at approximately 10:00 am local time. The deployment location was 32° 38.5' N and 79° 46.5' W (see Figures 1 and 3) situated to the west of the southern part of the western ODMDS berm.

The tripod was equipped with sensors measuring flow and sediment characteristics within the lower 1-meter of the seabed. In particular, flow conditions were measured at 41.5 and 43.5 cm above the seabed using two Sontek Acoustic Doppler Velocimeters (ADVs). The two sensors were horizontally separated by a distance of 87cm (i.e., approximately 2 times the distance above the seabed). Turbidity levels were measured using two Optical Backscatter Sensors (OBS) installed at approximately 31 and 50cm above the seabed. Two strain-gauge transducers were used to measure variations in hydrostatic pressure due to wave and tidal sea surface variation. The transducers were integrated within the ADV systems, which were equipped with heading, pitch and roll sensors used to obtain information on direction and inclination of the sensors. All data were synchronized and logged onboard an underwater data logger. Data were collected in a burst mode with one 12-minute long burst collected every 30 minutes. Sampling frequency within a burst was 10Hz resulting in 7,200 data points per channel per burst.

Figure 2. Photograph showing the Coastal Processes & Sediment Dynamics (CPSD) Laboratory tripod used for the data collection.

The deployment took place using the EPA R/V Anderson with the assistance of EPA divers. Originally, the tripod was scheduled to remain on location for a period of 15 days.

However, due to difficulties in securing a suitable vessel for the recovery, the tripod remained on the seafloor for a period of 35 days. It was recovered on August 20th, 2001 using the NOAA Ship Ferrel with the assistance of Center for Marine and Wetland Studies center from the Coastal Carolina University and a diving team from SCDNR.

The system stopped collecting information when the memory (total of 440MB) was filled with data. A total of 1,388 bursts were collected, corresponding to a period of 28.9 days.

2.2 Mapping of tidal currents over the ODMDS for a full tidal cycle.

A RD Instruments 1200KHz Workhorse Sentinel Acoustic Doppler Current Profiler (ADCP) was used to map the currents in the vicinity of the western disposal berm (for survey lines see Figure 3). The ADCP was mounted on the side of the R/V Anderson and data were transmitted real time and recorded to a computer onboard the vessel. Currents were measured continuously throughout the water column with a vertical resolution of 40cm. Mapping was conducted over a period of two tidal cycles during the period of July 6th, 11:00am to July 7th, 2001 11:00am.

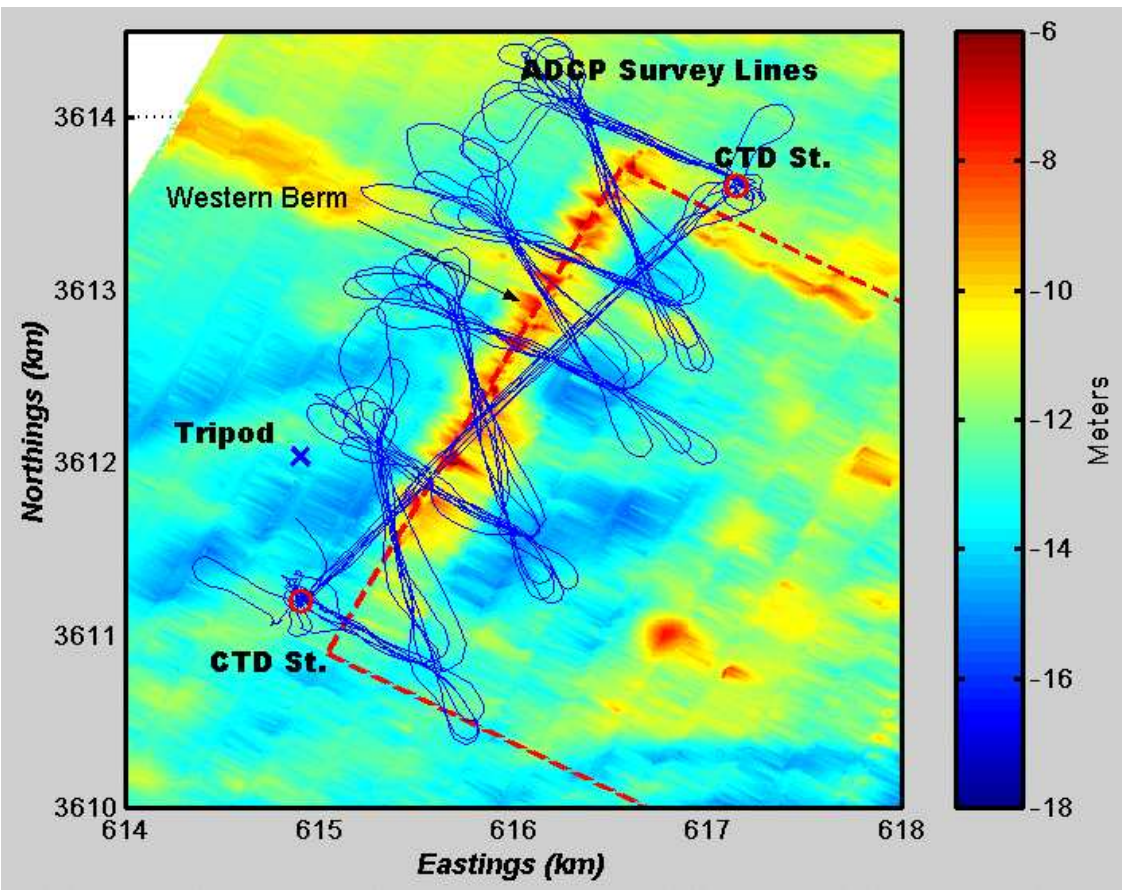

Figure 3. Detailed bathymetric map of the ODMDS (data from Gayes 2000) showing the western berm (shallow, hot colors) and the location of the tripod deployment (green circle). ADCP survey lines and locations of the CTD stations (red circles) in the NE and SW ends of the berm are also shown. The outline of the ODMDS is shown as a red, dashed line.

In addition to current measurements, 15 CTD casts were collected at two locations (at the NE and SW ends of the western berm, respectively, see Figure 3). These data were collected in order to evaluate the effect of the freshwater plume from Charleston Harbor in dispersing re-suspended sediment. No density gradients were found and thus these data will not be presented here.

Vessel position during the ADCP survey and CTD casts was obtained using a Differential GPS system.

2.3 Auxiliary Data

Additional data for the period of the field data collection included wind speed and direction as well as sea surface elevation data.

Wind velocities and directions for the instrument deployment period were obtained from the C-MAN station FBIS1 at Folly Island, SC (32.68 N 79.89 W), which is located approximately 12km northwest of the tripod deployment location and owned and maintained by National Data Buoy Center (NDBC) (Figure 1).

Sea surface elevation was obtained from the NOS tidal station (8665530) located in Charleston Harbor at 32° 46.9' N and 79° 55.5' W (Figure 1).

3. DATA ANALYSIS & RESULTS

3.1 Averaged Time-Series.

The data collected by the instruments located on the tripod were downloaded and split into individual files (i.e., one file for each ADV per burst) resulting in the creation of 2 x 1388 data files. The statistics (i.e., mean and variance) of the time-series from each file (i.e., burst) and for each channel were calculated and examined for “suspicious” values which usually correspond to noisy data or spikes. Spikes were found in the pressure data and were removed using a wild-point editing algorithm.

Subsequently to data quality examination, burst-averaged values of the three components of flow (in cm/s), pressure (converted to meters) and turbidity (in counts[1]) were calculated. Examples of the mean values of water depth, east and north components of near bed currents from one of the ADVs and OBS data from both elevations (31 and 50cm above bed) are shown in Figure 4. It is characteristic that both sea surface and current flow signals are influenced by the wind. Turbidity data from the OBS sensors were deteriorated after day 195 (deployment day 8) because of biofouling. The effect of biofouling is exhibited as a background level that gradually increases with time. After day 197 and 199 (deployment days 10 and 12) the return signal for the lower and upper OBS sensors, respectively, dropped to zero. This is because the whole surface of the

[1] The OBS was not calibrated. Counts are linearly related to suspended sediment concentration.

sensor was covered by growth resulting in the optical signal being completely blocked and thus no return signal was detected.

The OBS signal was corrected for the period of biofouling by subtracting the background level from the affected part of the data. The minimum OBS value over a 3-hour moving window was estimated and then subtracted from the raw data. The corrected OBS data are shown later in section 3.5.

Wind speed and direction from the Folly Island meteorological station for the period of the deployment are shown in Figure 5. Periods of strong wind activity correspond to periods of strong flow as shown in Figure 4 (for example, compare winds in Figure 5 with currents in Figure 4, for days 195, before 205 and after day 205). The high correlation between winds and current deviation from the tidal signal confirms the importance of the wind in the transport of mass in the coastal ocean in general and the study location in particular, as was indicated by Williams *et al*. (1987)

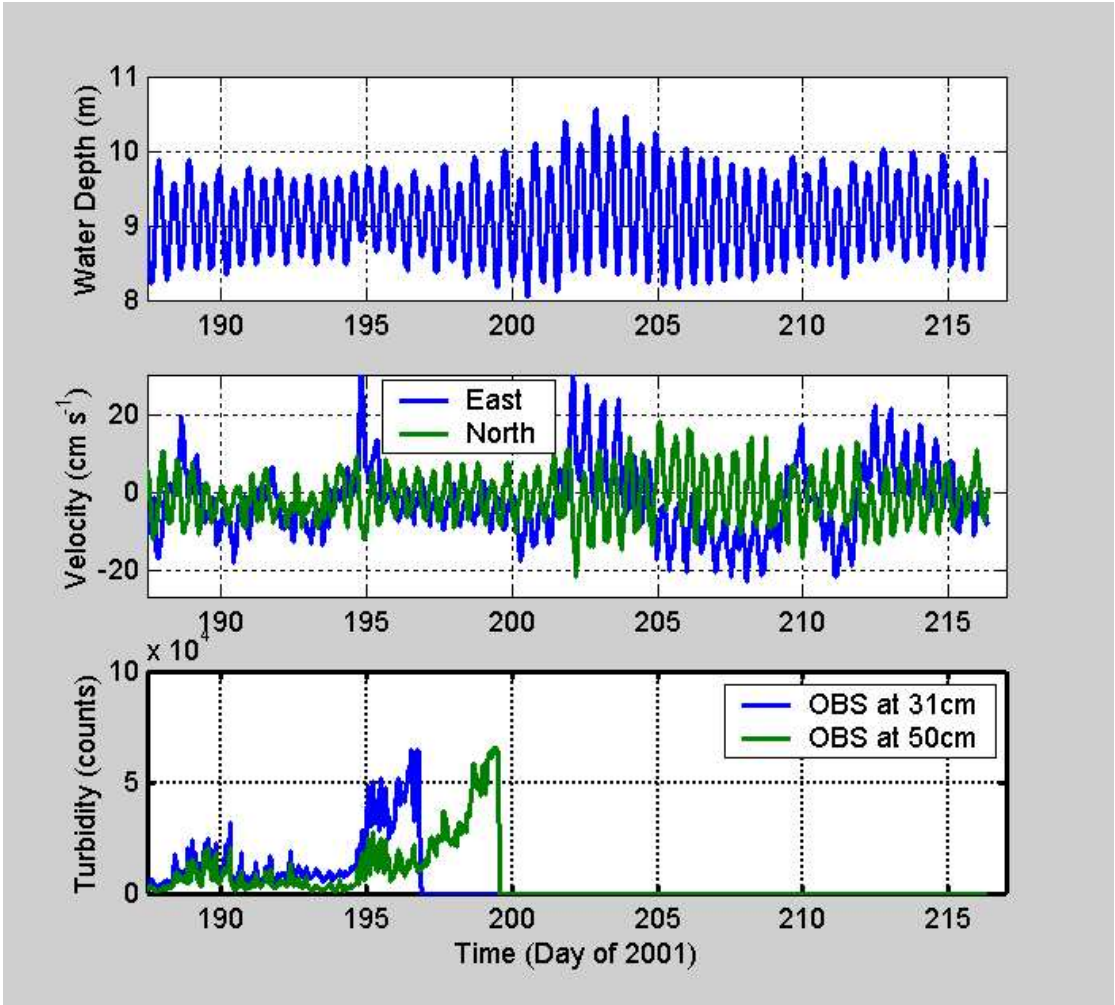

Figure 4. Time-series of burst-averaged values of local water depth (top panel), east and north components of flow (middle panel) and OBS-measured turbidity levels.Notice the turbidity level background increasing after day 195 (deployment day 8) due to biofouling.

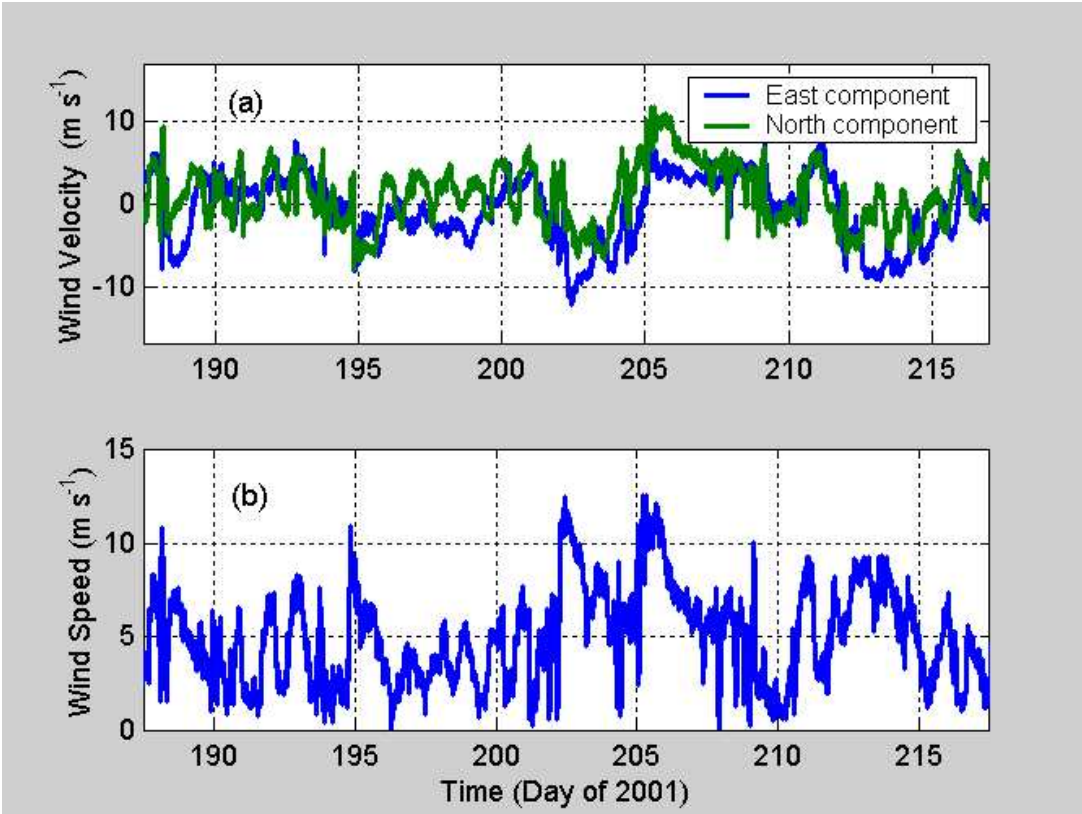

Figure 5. Time-series of: (a) east and north components of wind velocity (oceanographic convention) and (b) total wind speed for the period of the experimental data collection.

3.2 Tidal Analysis and Wind-Driven Flows.

The surface elevation and the current data collected by the tripod were analyzed in order to derive the amplitude and phases of the tidal constituents. The results of this analysis were used to separate the tidal- from the wind-driven flow.

The tidal analysis program used was developed at the Institute of Ocean Sciences in Canada by Foreman (1977). Amplitudes and Greenwich phases were calculated via a least squares method coupled with nodal modulation only for those constituents that could be resolved over the length of the record. The results of the Tidal Analysis are shown in Appendices I and II, for sea surface elevation and currents, respectively. The major constituents for sea surface elevation are the M_2, S_2 and K_1 with amplitudes of 73, 9 and 12 cm, respectively (see Appendix)[2]. As for the currents, the M_2 component is the most significant component with the M_{sf}, N_2, S_2 and O_1 being the other most important

[2] It should be noted that comparison of the tidal constituents at the site with those estimated using the NOAA NOS records at Charleston Harbor showed a difference on the M2 phase of 15degs. This means that tidal elevations at the ODMDS site occur approximately 30min earlier than measured at the NOAA NOS site in Charleston harbor. This should be taken into consideration when using the NOS data for correcting bathymetric data of the site for tidal variation..

components. The M_2 current ellipse of the near bed currents is oriented at an angle 13 degrees from north (see Figure 6). The tidal ellipses measured in this study are a little different than those found by Williams *et al.* (1987). These differences, however, might be expected since the two locations are some 4km apart, with the current study location in shallower water (for a comparison of the two locations see Figure 1).

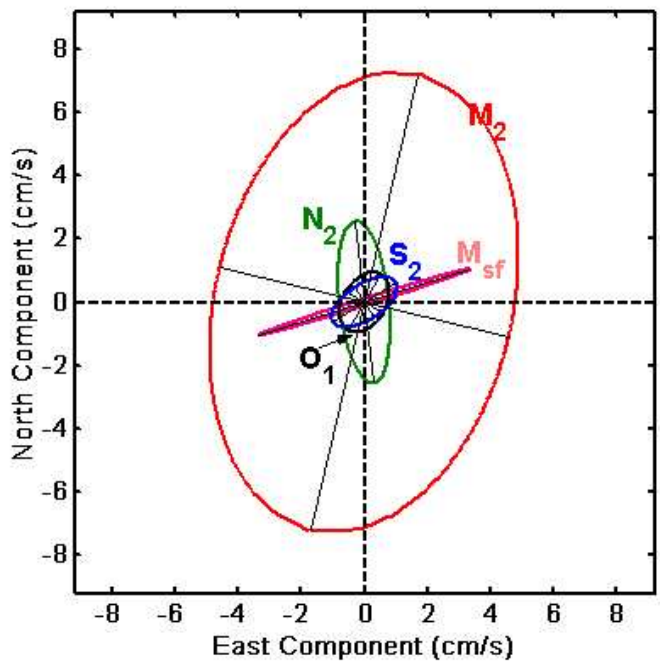

Figure 6. Near bed tidal current ellipses of the most important tidal constituents**.**

Figure 7 shows the tidal analysis of the sea surface elevation measured on the site. The measured sea surface elevation is decomposed into a tidal component (blue line) and a non-tidal residual sea surface variation (red line). The latter shows a super-elevation of the mean water level on days 195, 203, 210 and 213. These periods correspond to periods of NE wind conditions. It is characteristic that SW winds (see Figure 5, day 205) do not create any set-up (i.e., super-elevation) on the mean sea level.

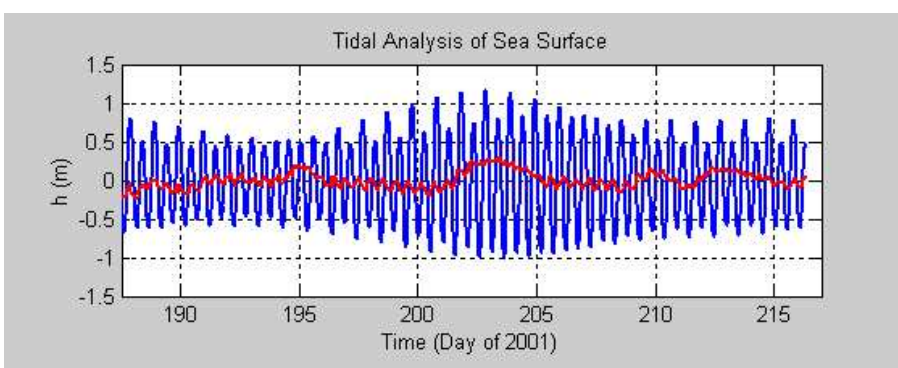

Figure 7. Results of harmonic analysis of sea surface elevation: (a) predicted tide (blue); (b) residual sea surface elevation due to wind forcing (red).

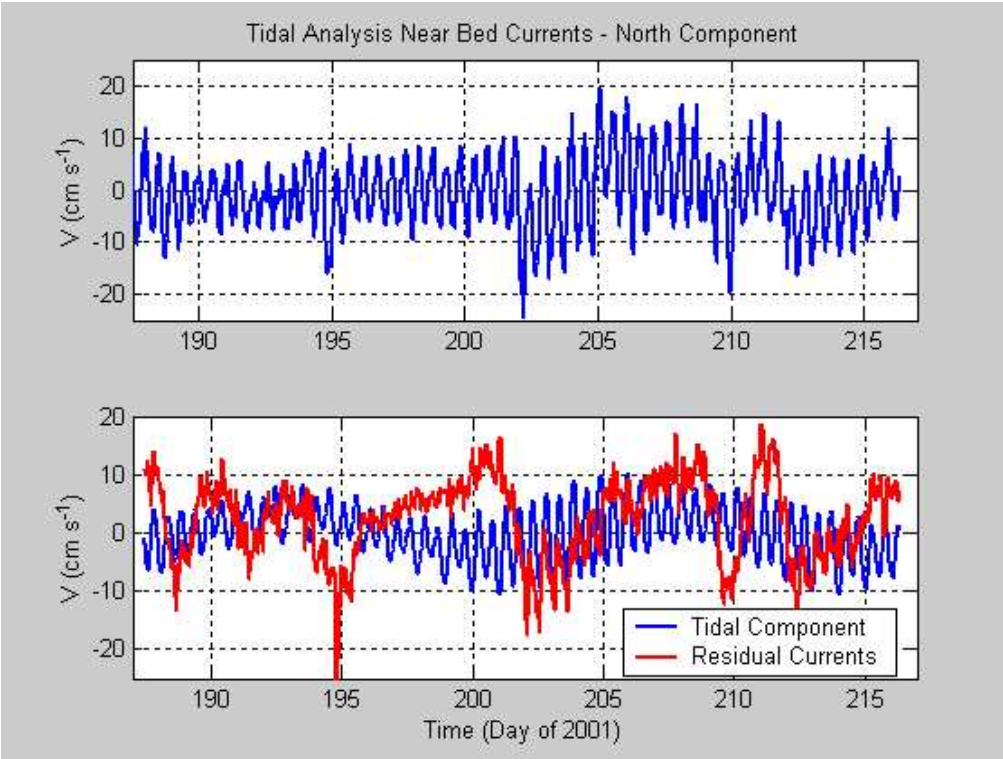

Figure 8. Results of harmonic analysis of the north component of the nearbed currents. Top: raw time-series. Bottom: predicted tides (blue) and residual wind-driven current (red).

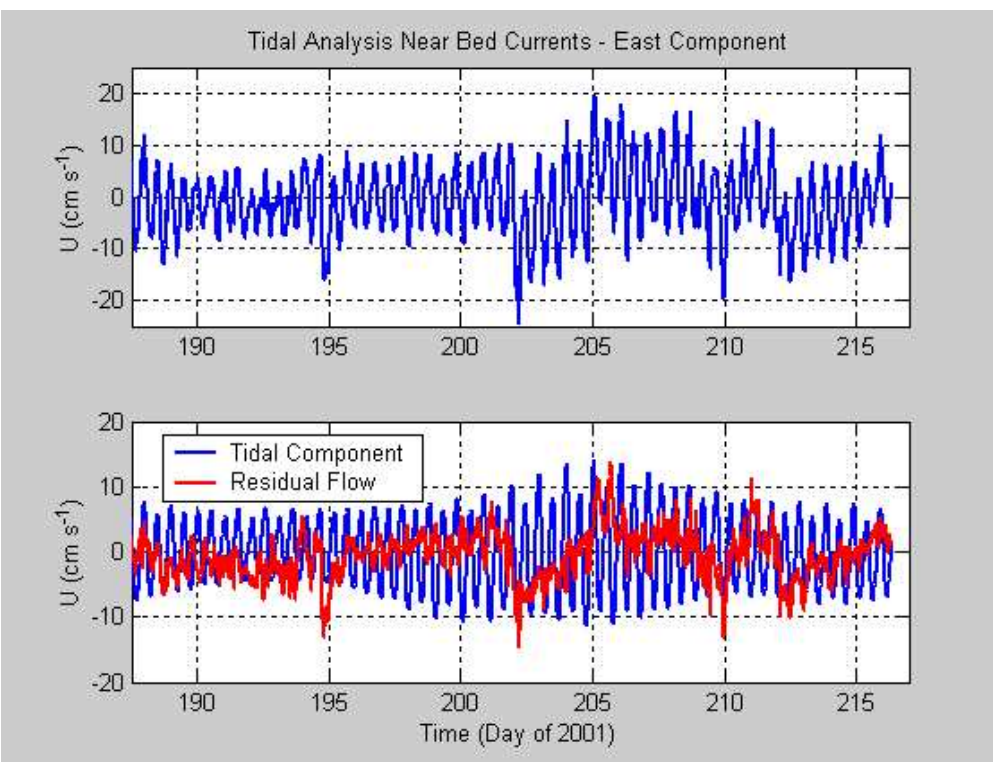

Figure 9. Results of harmonic analysis of the east component of the nearbed currents. Top: raw time-series. Bottom: predicted tides (blue) and residual wind-driven current (red).

The tidally-induced flow along the north and east directions as predicted by the tidal harmonic analysis are shown in Figures 8 and 9, respectively, together with the residual flow, which is defined as the difference between the tidal predicted component and the raw, measured data. Overall the total variance of the near bed current record was 113.6 cm^2/s^2, and the tides can explain only 46.2% of this variance. The tide was responsible for 70.3% and 30.2% of the total variance in the east and north components of flow, respectively.

The tidally induced flow along the north and east directions as predicted by the tidal harmonic analysis are shown in Figures 8 and 9, respectively, together with the residual flow, which is defined as the difference between the predicted tidal component and the measured data. Overall the total variance of the near bed current record was 113.6 cm^2/s^2, and the tides can explain only 46.2% of this variance. The tide was responsible for 70.3% and 30.2% of the total variance in the east and north components of the flow, respectively.

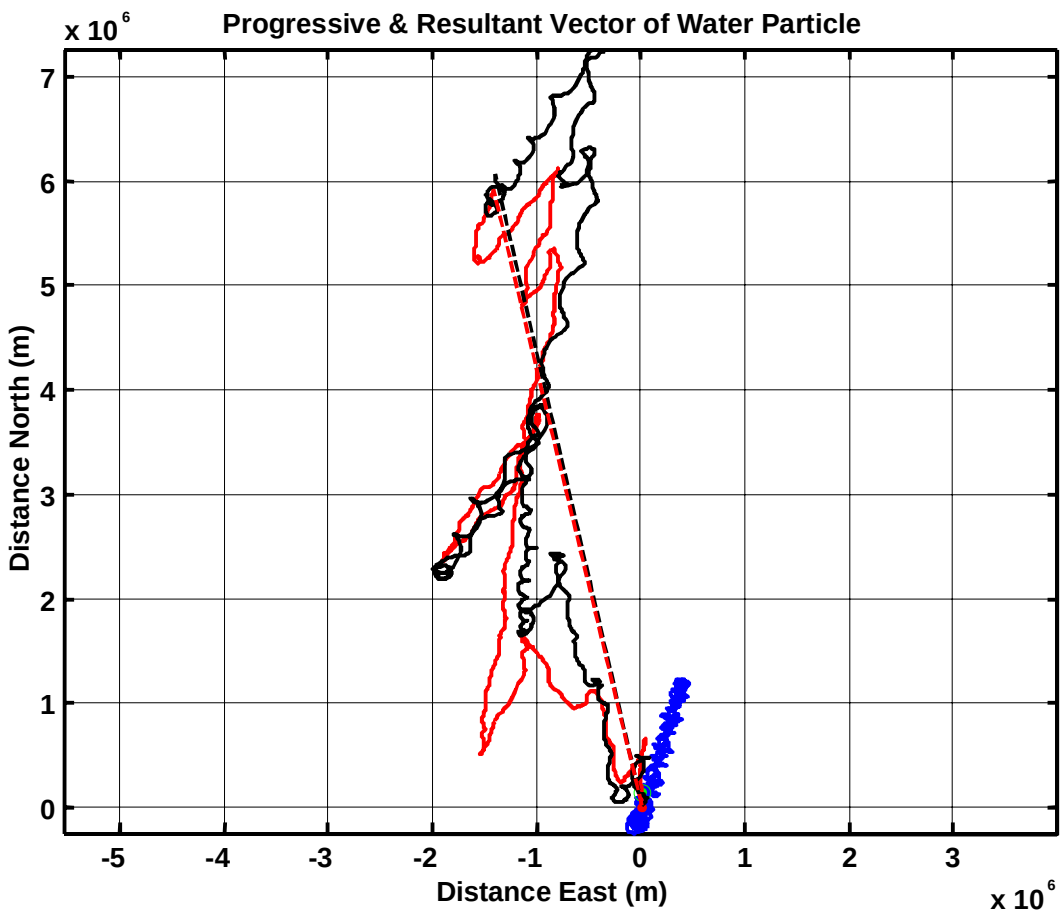

Figure 10. Progressive and resultant vectors for tidal (blue), wind-induced (red) and for combined tidal and wind-induced circulation (black) over the 28.9 -day period of data collection. The similarity in magnitude and direction of the resultant vectors for the case of wind only (red dashed line) and wind and tidal circulation (black dashed line) clearly demonstrate the importance of the wind driven circulation in transporting water masses in the study area.

The progressive and resultant current vectors for the deployment period and for the cases of (i) tidal current only; (ii) wind-driven flow only and (iii) wind and tidal flow are shown in Figure 10. It is striking that the tidal current does not contribute significantly in the net transport of water mass. Wind-driven circulation is the major contributor in moving water mass and sediment that might be in suspension in the water.

3.3 Wave Characteristics.

Significant wave height (H_s), wave bottom orbital velocity (U_b), wave period (Tp) and wave direction were calculated for each burst using the concurrent measurements of pressure, u and v components of the instantaneous flow (PUV analysis). Spectral estimates of pressure and velocities were calculated. The pressure spectra were converted into sea surface elevation spectra after correcting for wave attenuation with depth, according to the method described in Bishop and Donelan (1987). The total variances of sea surface (σ_h^2) and orbital velocities (σ_u^2 and σ_v^2) were calculated by integrating the sea surface and velocity spectra over the wave frequency band (0.02 to 0.5Hz).

Significant wave height and maximum bottom orbital velocities were estimated as $4*(\sigma_h^2)$ and $2*(\sigma_u^2+\sigma_v^2)$, where u and v are the two horizontal components of flow. Wave period was taken to be the peak period as identified in the spectra, while wave direction

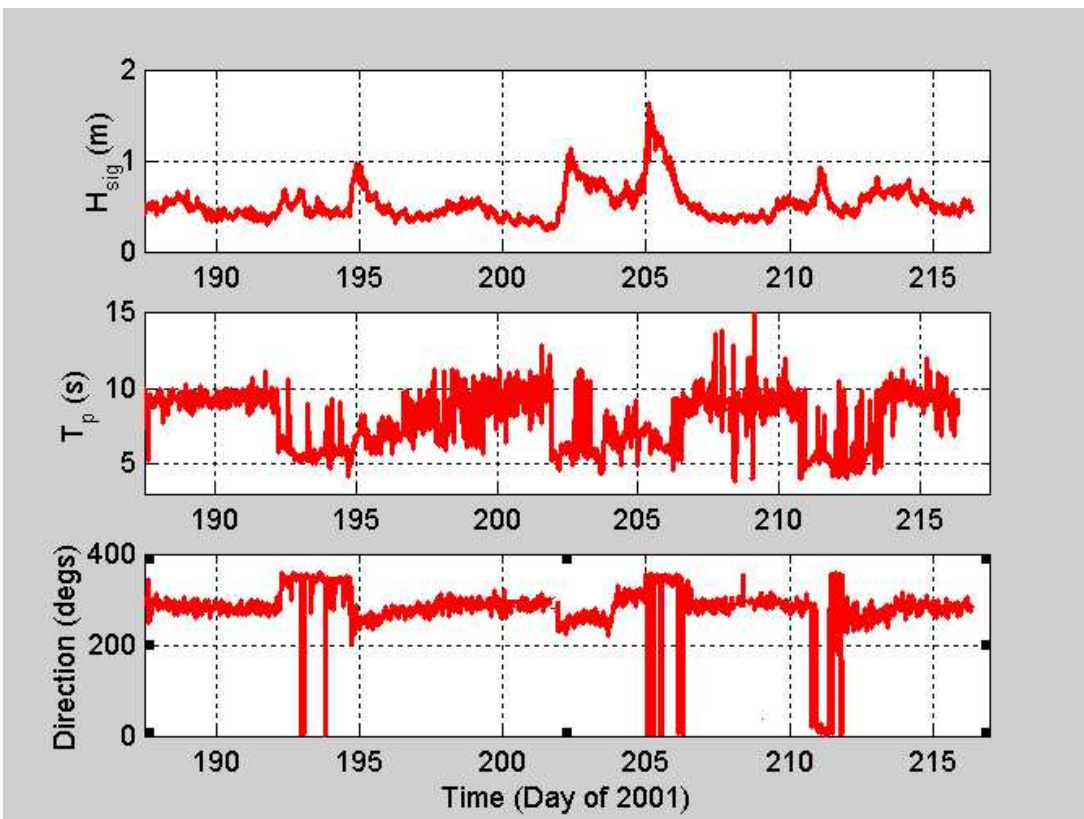

Figure 11. Time-series of wave characteristics as calculated from the spectral analysis of the pressure and velocity records.

was calculated from the co-spectra of the p, u and v time-series according to the method described in Earl and Bishop (1984)

The wave conditions as calculated for the period of the deployment are shown in Figure 11, while the wave climate is shown as a polar diagram in Figure 12.

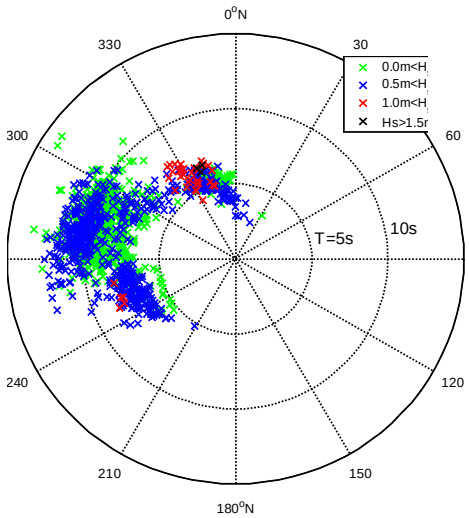

Figure 12. Polar-diagram showing the wave-climate for the period of the measurements. Dashed line indicates the general orientation of the coastline. The majority of the waves are mild with periods between 6 and 10 sec and a direction of approach from the ESE. Bigger waves (red crosses) occur during wind activity, are locally generated, have a wave period of approximately 5 to 7 sec and a direction from the south or the NE.

3.4 Bottom Stress Estimates

The forces exerted on the seabed drive the motion of the sedimentary particles. These are the shear stresses due to mean (tidal and wind-driven) currents, and wave, oscillatory motion. Although methods exist for the direct measurement of the stresses due to steady currents, the estimation of wave-induced shear stresses still relies on the application of numerical or analytical models.

Shear stress estimates in the constant stress layer can be obtained using the law of the wall, the inertial dissipation (ID) or the Reynolds stress techniques. The latter method is the most desirable since it provides a direct estimate of the shear stress. However, it requires concurrent measurements of the 3-D flow field. Further, when waves are present, as is the case at the ODMDS, the technique is sensitive to alignment of the sensor in relation to the local bed. The ADV can provide accurate information on the 3-D flow field, and under steady flow conditions the Reynolds stress estimates are accurate within 1% (Voulgaris and Trowbridge, 1998). However, when waves are present, any error in sensor alignment in relation to the local seabed produces large errors in estimates of

Reynolds stress. In such conditions, the wave contamination can be removed using two sensors displaced horizontally (Voulgaris et al. 1997, Trowbridge 1998).

In this deployment, the two ADV sensors (1 and 2 respectively) were displaced horizontally by a distance of approximately 87cm. Thus, the Reynolds stress (<u'w'>) was estimated as (Voulgaris et al. 1997; Trowbridge 1998):

$$< u'w' >= \frac{1}{2} < (u_1 - u_2)(w_1 - w_2) > \qquad (1)$$

where u and w are the instantaneously measured downstream and vertical components of flow, respectively. The subscripts 1 and 2 denote instantaneous velocity values measured by the two horizontally separated sensors. The mean bottom shear stress is related to the measured Reynolds stress as follows:

$$\tau_c = \rho < u'w' > \qquad (2)$$

Another method that was utilized in the analysis of the data is the inertial dissipation method. It assumes the existence of an inertial sub-range over which energy is cascaded from turbulence producing low frequencies to turbulence dissipating high frequencies. This method is based on the premise that the energy production and dissipation ranges are well separated and that the spectrum between these two ranges follows a universal -5/3 Kolmogorov Law (Tennekes and Lumley 1989).

Thus, the spectrum of the vertical component of flow for each burst was calculated, and the shear velocity (u_*) was estimated by applying the following equation to the inertial sub-range region:

$$u_* = (\kappa z)^{1/3} \left[\frac{F_{33}(k) k^{-5/3}}{\alpha_3} \right]^{1/2} \qquad (3)$$

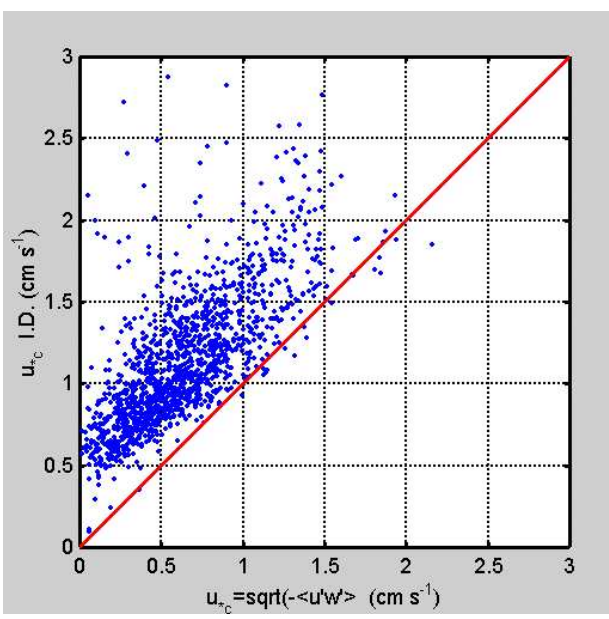

Figure 13. Comparison of mean current shear velocities estimated using the inertial dissipation (ID) method and the Reynolds stress technique. The 1:1 line is also shown for reference

where κ is the Von Karman constant (=0.4), $F_{33}(k)$ is the spectral density of the vertical component of the flow at the wave number k (=2π<u>/f, where f is spectral frequency and <u> mean downstream flow speed).

Time series of mean current shear velocity estimates from both methods are compared in Figure 13. Estimates of shear velocity derived with the inertial dissipation (ID) method were higher than those derived using the Reynolds stress method. The over-prediction of the ID technique was greater for smaller shear velocity values (weak current conditions). This discrepancy is attributed to

contamination of the spectra by (i) noise and (ii) wave energy that leaks into the inertial dissipation range of the spectrum. The Reynolds stress technique, when applied to data collected with an ADV sensor, is immune to noise levels (see Voulgaris and Trowbridge, 1998). Further, the use of a pair of synchronized sensors and application of the differencing technique (as applied here) removed the effect of the waves, ensuring a better estimate of Reynolds stress and shear velocities. Thus, the Reynolds stress values obtained using Eq.1 are considered to be most accurate and representative of the environmental conditions that occurred during the experiment.

The Reynolds stress-based shear velocity values are related to the mean velocity measured at z=40cm in Figure 14. From the correlation of the square of the two values, we obtain the drag coefficient for the study location defined as $Cd=u_*^2/U_z^2$. When Cd is calculated at z= 40cm, the result is 0.0039. This value translates to a Cd=0.001 at z=100cm, which is an elevation commonly used to express drag coefficient values.

The Reynolds stress based values of shear velocity were used to evaluate the results of the modeling efforts described below.

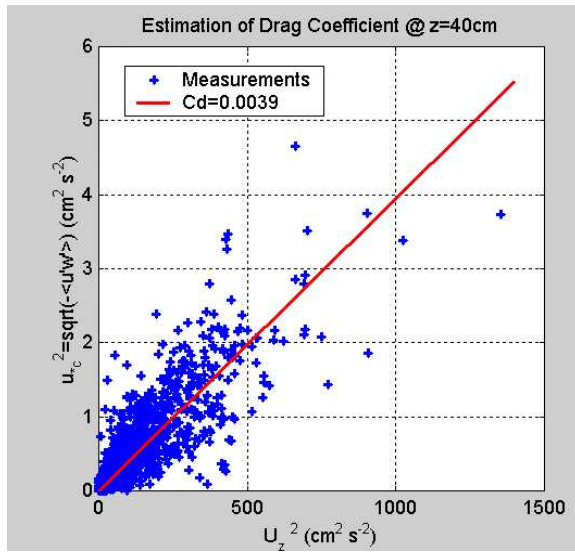

Figure 14. Estimation of bottom drag coefficient, Cd, from the Reynolds Stress derived mean shear stress.

3.5 Modeling of Hydrodynamics and Suspended Sediment Transport.

The shear velocities estimated using the Reynolds stress method correspond to those due to the mean flow (tidal and wind-driven). Wave-induced stresses are very important in setting the bottom sediment into suspension. Once in suspension, the mean currents are then carrying the sediment. Despite the importance of the wave-induced shear stress, no method exists for directly measuring it in the field. Instead, we have to rely on numerical or analytical models. In this study, the wave-induced stresses and the combined wave and mean current shear stresses were estimated using the 1-D vertical model developed by Styles and Glenn (2000).

The input parameters for the application of the model are, wave bottom orbital velocity (Ub), wave period (Tp), mean current speed (Uz) and direction at a reference elevation (z=40cm here) and relative angle of waves and currents.

All of the above parameters for input in the model were calculated using the data collected with the bottom tripod. The model predicts the bottom morphology (ripples) as a function of the hydrodynamic forcing, and then calculates the mean current's shear

stress, the wave-induced shear stress and the combined maximum wave and current shear stress. The model also utilizes a sediment pick-up function to calculate the sediment resuspension and suspended sediment transport. The model is 1-D and does not include any advection of sediment. It assumes bottom morphology in equilibrium with the flow and sediment exchange only in the vertical. Sediment characteristics are included in the model as sediment size per fraction and percentage of each fraction on the seabed. Ten sediment fractions were used in the analysis, determined from sieving sediment samples taken from the site. These are shown in the table below:

Class #	Particle Size (mm)	Percentage (%)
1	500	5.0
2	350	4.0
3	300	3.0
4	250	4.5
5	210	12.0
6	180	16.0
7	150	31.0
8	130	16.0
9	110	6.0
10	90	2.5

Table 1. List of the particle size fractions and their corresponding frequency of occurrence as used in the sediment resuspension and transport model**.**

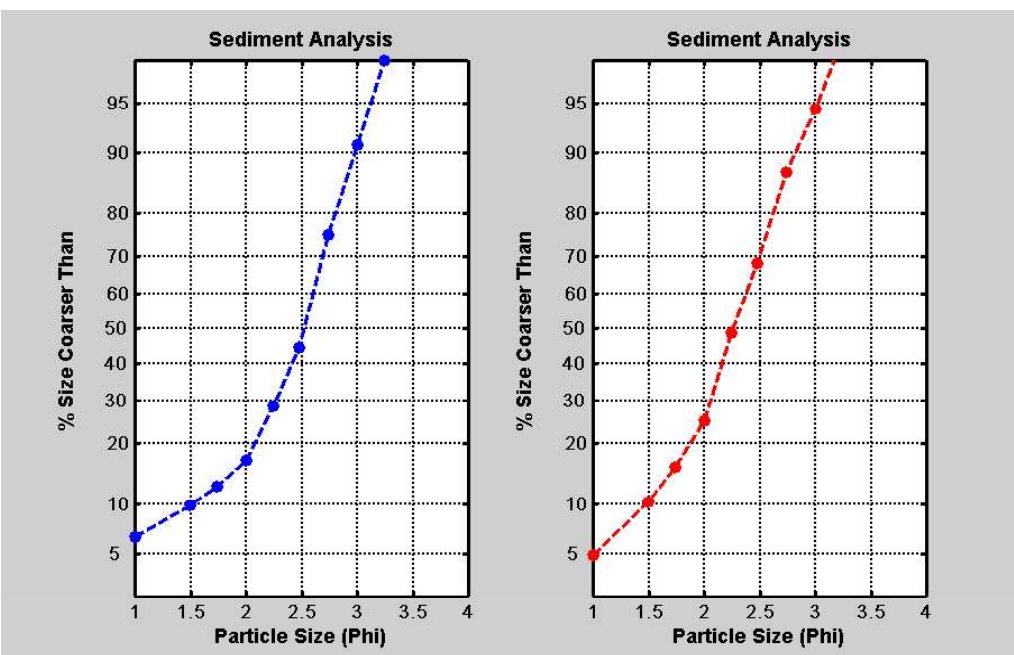

Figure 15. Particle size analysis results for bed sediment samples collected from the tripod deployment site (right) and the western berm location (left). Notice the slightly higher percentage of fines found over the berm. (Note: particle size units are in Phi where Phi=-$\log_2$(d in mm)).

At this juncture, it should be noted that the model is valid for non-cohesive sediment. The sediment samples obtained from the seabed by the divers were non-cohesive; however, a large percentage of the material disposed in the area is fine, cohesive material, which will have different hydraulic behavior than that of non-cohesive material. The particle size analysis of the sea bed sediment samples (Figure 15) shows that at least 5% of the material is silt and/or clay, with a slightly higher percentage of fines found over the berm.

The model-predicted mean and combined shear stresses are shown in Figure 16. A comparison of the model-predicted mean shear stress with the value measured with the ADVs is shown in Figure 17. The model seems to under-predict shear velocities during high energy and over-predict at low energy conditions. This is attributed to the fact that the model uses equilibrium conditions between flow and mobile bed for the establishment of bed roughness. Nevertheless, the overall agreement is satisfactory for the purposes of establishing sediment transport pathways.

Figure 18b shows suspended sediment concentration at an elevation 40cm above the bed as predicted by the model. This is compared to the (non-calibrated, corrected for biofouling) OBS measurements (Fig. 16a). The largest resuspension event was observed on day 195 when the wind speed was 10m/s and direction from the SW. The waves were 1m in height, 8s in period and were approaching from the WSW. The other two major resuspension events occurred at the start of the data collection (day 189) and at the end of the period of useful OBS data collection (days 197 to 200). The same events were predicted, in a qualitative manner, by the model. However, the major difference between

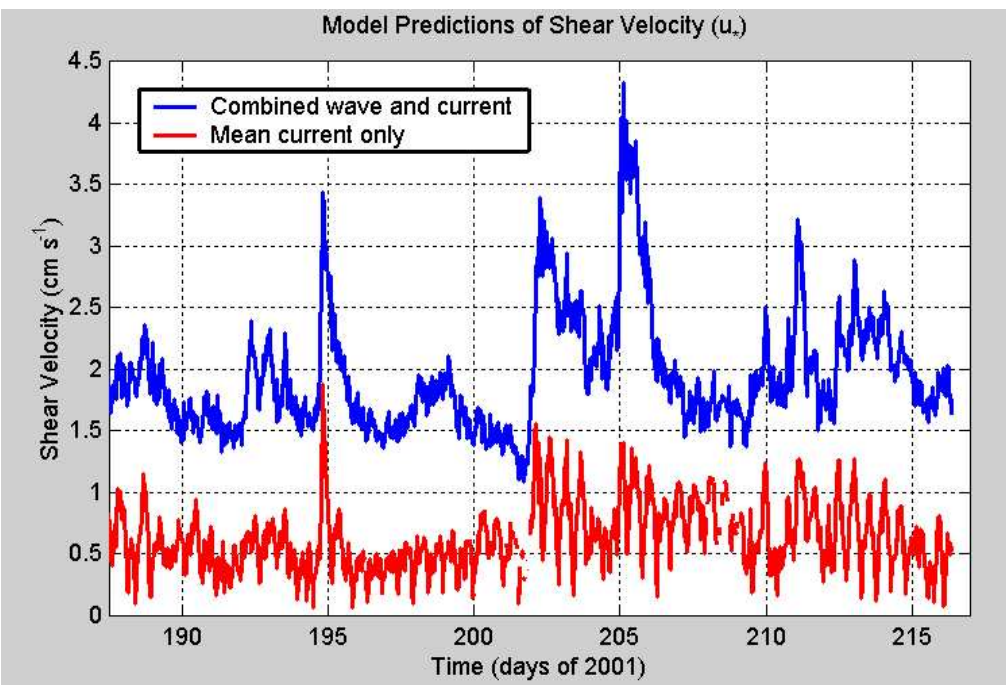

Figure 16. Model prediction of mean current shear velocity (blue) and maximum combined wave and current shear velocity (red). Notice the contribution of the waves significantly increases the bottom shear velocity and thus contributes more to sediment mobility

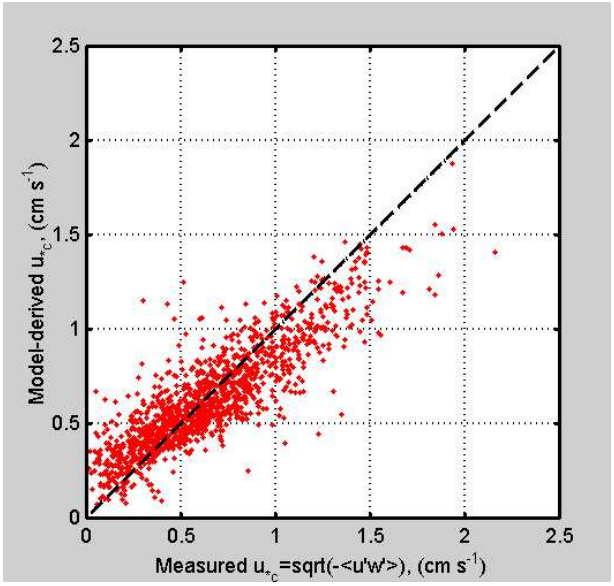

Figure 17. A comparison of the measured mean shear velocity to shear velocity as predicted by the model. The model appears to slightly under-predict shear velocities at high-energy conditions and to over-predict at low energy conditions. However, the overall agreement is satisfactory for the purposes of establishing

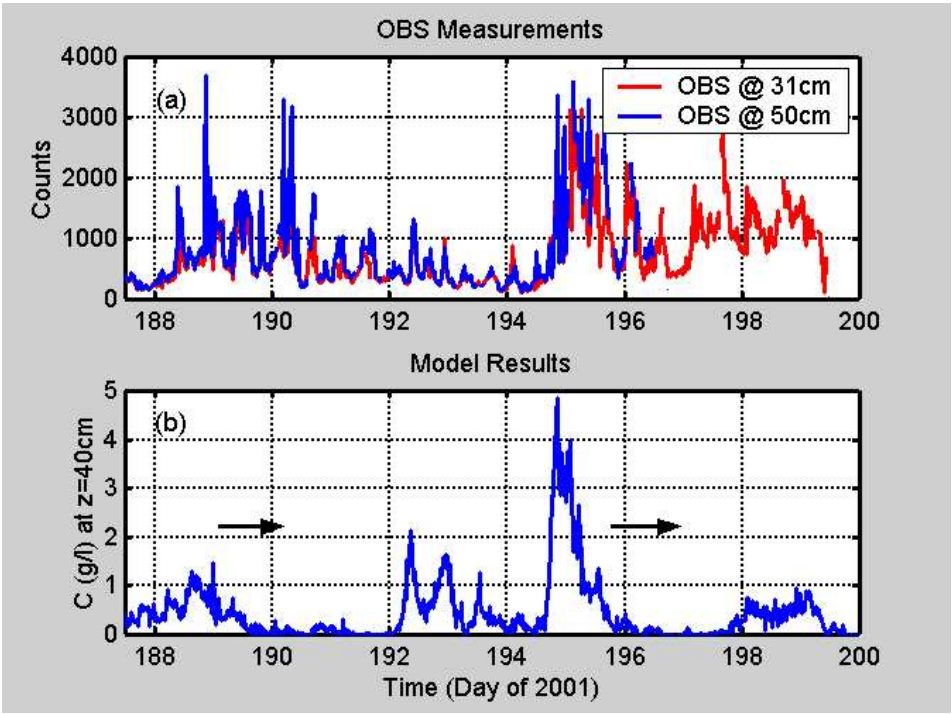

Figure 18. (a) Measured turbidity in the field using the OBS. Counts are linearly related to the amount of sediment in suspension in the water column. (b) Suspended sediment concentration as predicted by the model for the period of OBS measurements. Four major resuspension events are captured by the model (see days 188-190, 192-194, 195-196 and 198-200). The same events can be seen on the measurements but they are less distinct. The blurring of the events shown in the measurements is due to advection and to fine material being in suspension for a long time. The arrows on (b) are indicative of how advection of fine material from a resuspension event will be advected to elevate suspended sediment concentration levels at other times as indicated by the measurements.

the observed and predicted resuspension events is that the former persisted for longer periods (up to 2-3 days), while the latter ceased to occur within one day or as soon as the energetic conditions (high winds and currents) stopped acting on the area. The explanation for this discrepancy between measured and predicted sediment resuspenion levels lies with the fact that the model is one-dimensional and does not include advection. Also, there is some very fine, cohesive sediment in the area with settling velocities much lower than those used in the calculations. Following an energetic event, the fine material remains in suspension and is advected by the mean flow during the relaxation period. Bonding of the fine particles through flocculation processes might work toward acceleration of sediment deposition through the increase of the settling velocity. However, studies of fine sediment resuspension in oceanic conditions (Hill at al 2001), were waves are almost always present, have shown that the increased turbulence inside the wave boundary layer tends to break up the flocs and resuspend the sediment in the water column. According to this model, although the mean flow that was set in response to the wind field relaxes soon after the wind speed reduces, the waves will continue acting on the area for some time, breaking the flocs and maintaining the resuspension of the fine material. The one-dimensional model does not capture this. Instead, the development of a 2-D model is required to accurately represent the effects of advection in suspended sediment transport. The arrows drawn on Figure 18b indicate the advection of sediment that got resuspended during major resuspension events towards times with low predicted suspended sediment. Addition of this advective sediment would have made the predicted time-series of Figure 18b resemble those of Figure 18a.

The model also predicted suspended sediment concentration profiles. These were coupled with the mean velocity profile throughout the whole water column and then depth-integrated to generate a total suspended sediment transport vector. The predicted suspended sediment transport vectors, for the period of useful OBS data (up to day 199)

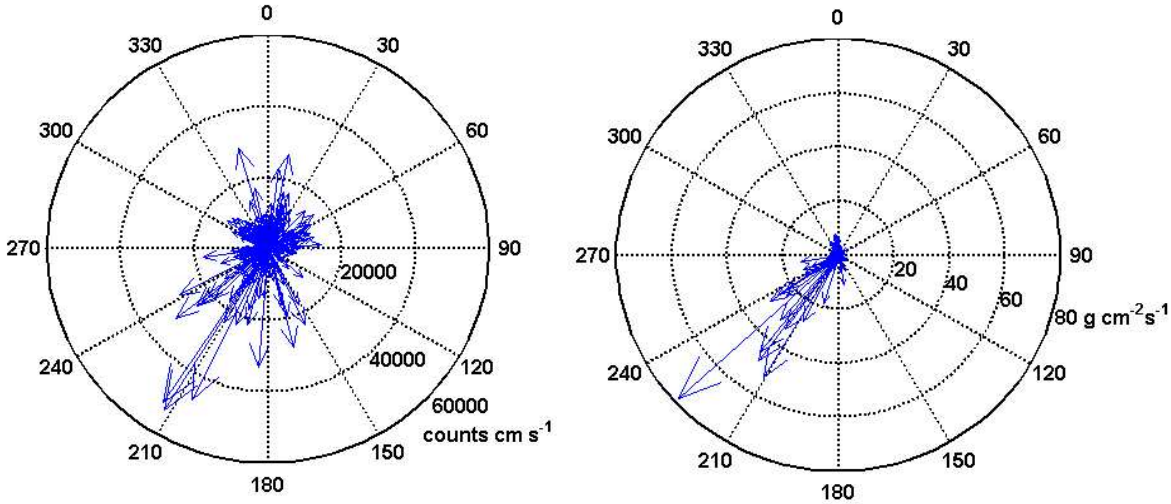

Figure 19. *Left Panel*: Local suspended sediment flux as measured at 40cm above the bed during the period of the deployment using data not affected by bio-fouling. *Right Panel*: Depth-integrated suspended sediment flux as predicted by the model assuming no-cohesive material and for the same period as in the left panel. (Note: count is the recorded output of the OBS sensor and it is a linear proxy of suspended sediment concentration).

are shown in Figure 19 (right panel) as a polar diagram. In the same figure (left panel) measured local near bed fluxes of suspended sediment are shown for comparison. Both measured local fluxes and predicted depth-integrated suspended sediment transport rates agree in that the major transport events contributed to a SW directed sediment transport. These fluxes correspond to moderate, locally generated wave activity (1m wave height, 5s period, NE direction) and wind (NE direction 10m/s wind speed) that produce a SW flowing current. The predicted sediment transport is dominated by this event. However, the measured fluxes (Figure 19, left panel) indicated that sediment was also transported in various other directions. As discussed earlier, this is because the fine material remains in suspension for long time after the resuspension event, and is advected by the currents that follow the event or by the currents of smaller events not capable of producing big resuspension events.

This problem must be addressed by a study of the sizes of material that are in resuspension during the actual resuspesnion event and at subsequent times. A study of concurrent monitoring of particle size and concentration is required to confirm the above expressed argument. Existing laser diffraction instrumentation (LISST-100, Sequoia Scientific Inc.) might be suitable for such a study. This should be accompanied by 2-D modeling of sediment transport that includes the advective component of the sediment.

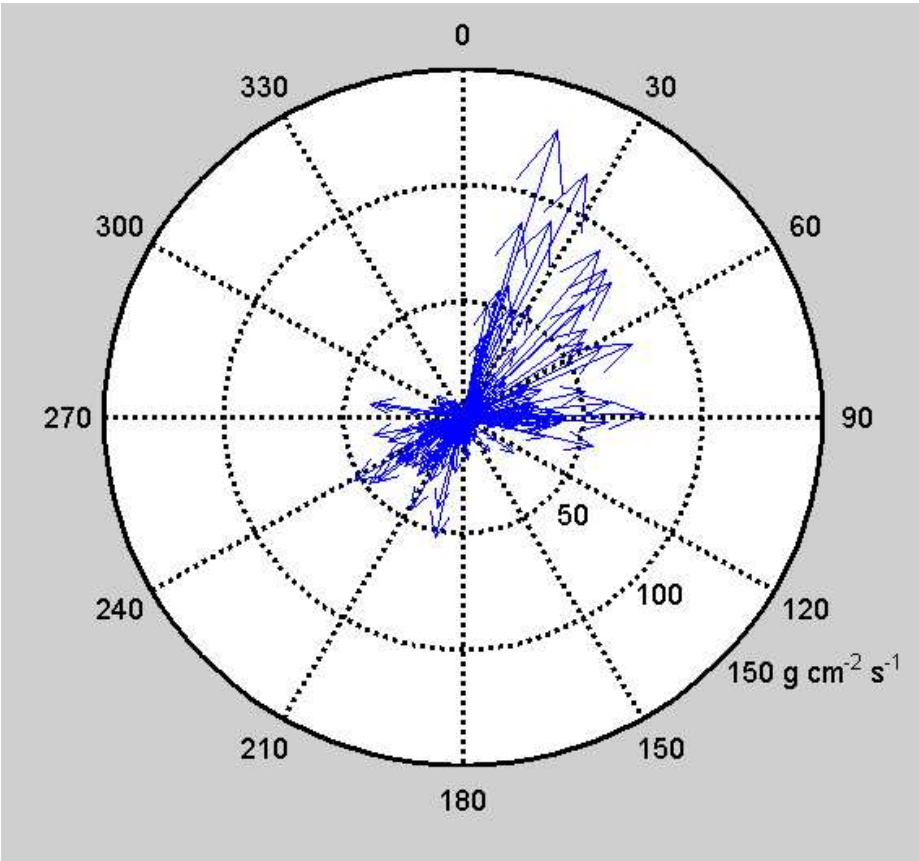

Figure 20. Depth-integrated local suspended sediment transport vectors predicted by the 1-D model under the combined action of waves and currents for the whole period of data collection. The sediment is transported into major directions NE and SW while minimal transport is predicted toward the shore or away from it.

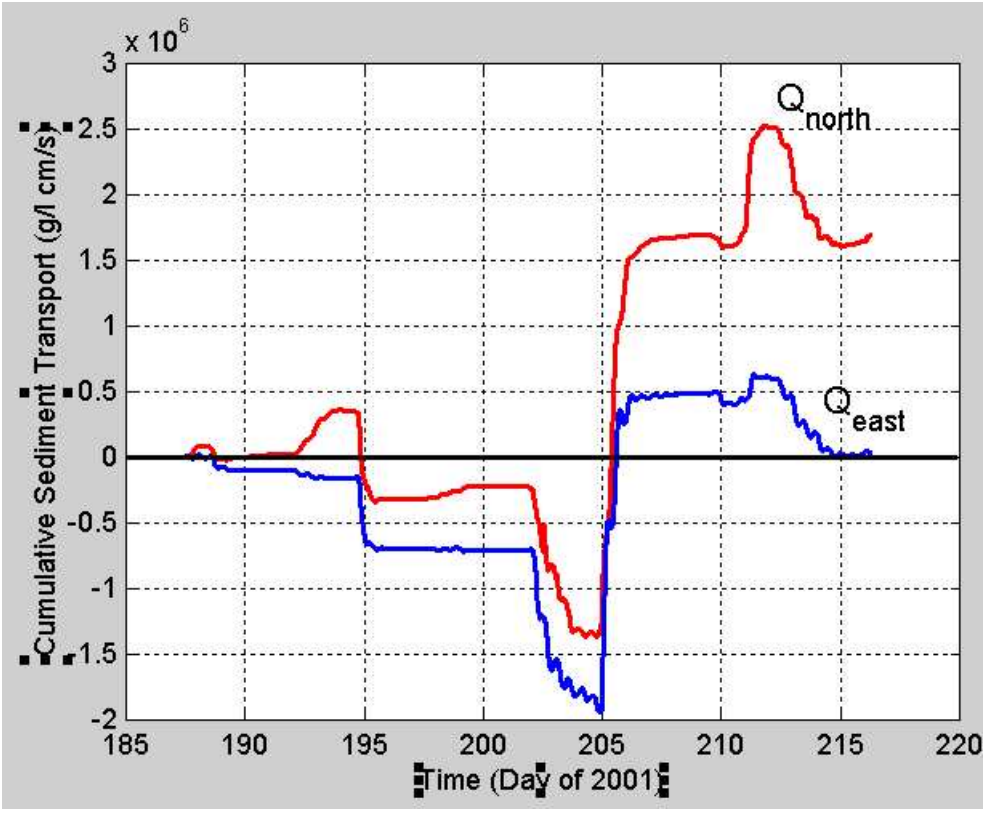

Figure 21. Cumulative sediment transport over the period of data collection.

Figure 20 shows the predicted depth-integrated suspended sediment transport for the whole period of the deployment. This figure shows that the biggest sediment transport events (excluding advection effects) were directed toward the NNE. Other events contributed to material being resuspended and transported in a SW direction. The event of day 205 was characterized by 13m/s wind speeds from the SSW, producing strong NE flows. This event was accompanied by waves 1.6m in height, 7s in period approaching from S. This event was the main contributor of this NNE sediment transport.

Calculation of the cumulative suspended sediment transport rate (i.e., the total effect of the sediment mobilization and transport over the data collection period, ignoring advection effects) was carried out and is shown in Figure 21. The sediment was transported over the data collection period in a net northward direction. The same figure shows that the sediment transport is rather episodic in response to the biggest events (see abrupt changes in values on days 195, 202.5, a reversal of net sediment transport on day 205 slightly enhanced further by an event on day 211). The events on days 205 and 211 correspond to winds from SSW, waves from S and a NE mean flow. The events shown on days 195 and 202.5 correspond to NE winds producing SW flows. It is anticipated that inclusion of advection would result in slightly reduced net transport of sediment, and it would also enhance dispersion of the sediment in the vicinity of the study area.

The above paragraph describes the sediment transport patterns during the study period. It is clear that such transport is controlled by the wind-driven flow. Wind data from the

Folly Beach station were statistically analyzed in terms of frequency of occurrence per direction and for different groups of wind speeds. Over 149,000 hourly values of wind data (speed and direction) collected during the period 1984-1991 were arranged in four groups based on wind speed ranges. The first group with wind speeds between 0 and 5 m/s is the most common with 90,867 (60.8%) of the occurrences. Winds with speeds between 5 and 10 m/s occur for 36.5% of the time (54,593 recorded occurrences), while the other two groups (wind speeds between 10 to 15 and greater than 15m/s) occur very rarely (2.6% and 0.1% of the time). Wind directions were converted from the meteorological (direction the wind comes from) to the oceanographic convention (direction the winds go to). Rose-diagrams of number of occurrences of wind events per wind direction, for each wind speed group, are shown in Figure 22. A similar rose-diagram together with a histogram of wind speeds for the wind conditions during the period of this study (28.9 days) are shown in Figure 23.

Figure 22 clearly demonstrates that there are two dominant wind directions in the ODMDS site: NE and SW winds. These winds drive flows in a SW and NE direction, respectively (see upper panel in Figure 22). The occurrence of SW winds (NE flows) is slightly higher for the most common wind conditions (0 to 10 m/s) occurring 97.3% of the time. Winds from the NE appear to be more dominant during very high-energy events (>10m/s) and occur only 2.7% of the time. The latter suggests that sediment transport during these high-energy events will be very intensive and directed toward the SW. Given the non-linearity between wind, flow and sediment transport it is not possible to extrapolate the wind percentage of occurrence to a sediment transport rate percentage of occurrences. This would require specific sediment transport climate analysis that utilizes the wind climate to predict wave and steady flows and then calculate sediment transport rates.

Wind speeds during the study period ranged from 0 to 12m/s (Figure 23). Most of the time the wind was from SW driving NE flows, while a few occurrences of eastern winds were recorded that drove W flows. The dominance of the SW winds explains the net northward sediment transport shown in Figure 21. Comparison of the data shown in Figures 22 and 23 suggests that the results of the measurement program were representative of the effect of the most common SW wind and wave conditions in the site. However, no significant events with winds from the NE were recorded. This suggests that in addition to the northern transport recorded during the study period will be significant sediment transport toward the SW. The intensity of this transport will be greatly dependent upon the wind intensity.

Qualitatively, the wind data suggest that major sediment pathway is along a NE - SW axis with the NE directions dominating over the year. Extreme events appear to favor sediment transport toward the southwest. Definition of a more accurate sediment transport “climate” requires the collection of more data under NE wind conditions and during some extreme events and extensive modeling over longer times.

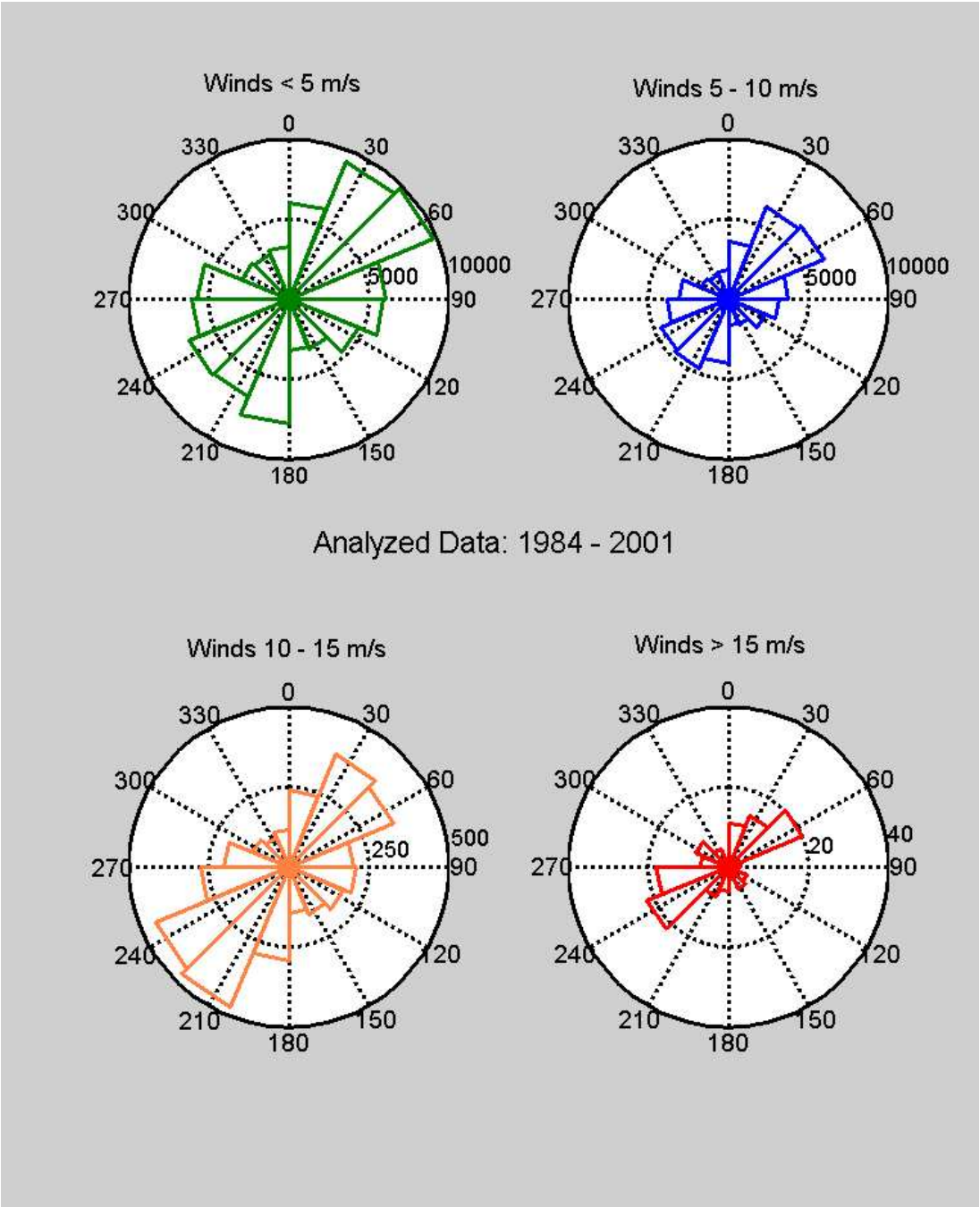

Figure 22. Rose-diagrams of wind direction (oceanographic convention) from the NOAA NBDC Folly beach meteorological station, for four different groups of wind intensity. The data analyzed to produce these diagrams were hourly wind speeds and directions covering the period 1984 to 2001. The numbers shown on the co-centric grids are number of occurrences.

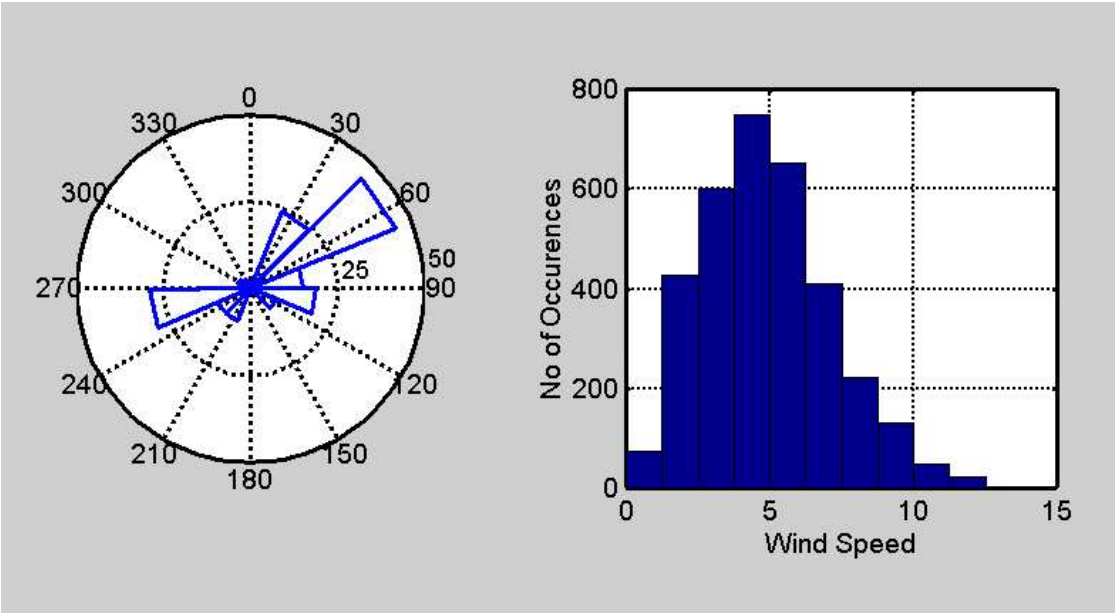

Figure 23. Rose-diagram of wind direction (oceanographic convention) and histogram of wind speed, from the NOAA NBDC Folly beach meteorological station, for the 28.9-day period of this study.

3.6 Mapping of the mean current field around the berm.

Analysis of the ADCP survey data for the 24-hour period of measurement showed that the current velocities over the western berm of the ODMDS followed a similar pattern as the currents in the stationary record. In particular, the currents tended to be heavily influenced by the wind direction in a similar pattern as was observed in the tripod data. During the period of the survey, a southwesterly wind induced a flow that produced an enhanced NE flow during the flood, and a weak NE flow during the ebb stage of the tide. The 24-hour record is too short and heavily influenced by the wind-driven component to reveal the existence of any topography induced mean flows over the western berm.

4. CONCLUSIONS

Based on the measurements and the modeling analysis that were carried out as part of this study we conclude that:

- Flow circulation and sediment dispersion appear to be both tidally and wind driven.
- Wind-driven circulation is the most important in controlling sediment transport. Strong winds generate waves that steer the sediment on the seabed and create large nearbed suspended sediment concentrations. The winds also drive wind-driven flows that transport the resuspended sediment along the direction of the mean current.
- High correlation of wind data from Folly Island and near bed flows suggests that the meteorological data can be used as a first order approximation of transport pathways

(near bed). Based on the sediment characteristics as measured, any wind-event is capable of resuspending and transporting sediment.

- Suspended sediment transport is directed mainly NE and SW in response to local wind climate and the wind-generated alongshore flows. During the measurement period the NE transport dominated the signal. This transport direction appears to be parallel to the direction of the main western berm thus questioning its effectiveness in trapping sediment. This direction is typical for the area. However, analysis of 8 years of wind data revealed that more sediment transport towards SW should occur in response to NE winds, which were very week during the study period. In any case, given the NE-SW sediment transport direction, the construction of the northeastern berm (bathymetric high in Figure 3) might be more effective in confining some of the sediment.
- Fine particles appear to be in suspension for the majority of the time, and in particular following a resuspension event. The low settling velocities allow them to be in resuspension for long periods (over 24 hours). Flocculation might assist settlement, but would be inhibited by the presence of the wave boundary layer, which is constantly present in the area (Hill et al. 2001).

5. RECOMMENDATIONS

- We recommend monitoring the particle size distribution of the suspended sediment as well as the concentration at three locations: SE of the ODMDS, inside the ODMDS and NE of the ODMDS. This approach will reveal the effectiveness of the berms in trapping sediment and develop priorities in disposal management and berm construction. The monitoring effort should include measurements of size fractions of sediment in suspension using appropriate techniques such as laser backscatterance and diffraction.

- Further, we recommend the development of a 2-D circulation and sediment transport model that incorporates the effects of advection in sediment transport pathways and the wind field at the ODMDS.

ACKNOWLEDGEMENTS

We would like to acknowledge the crews of the R/V Anderson and NOAA Vessel Ferrel for their assistance with the instrument deployment and recovery, respectively. Paul Gayes and the staff of the Center for Coastal and Wetland Studies of the Coastal Carolina University are thanked for providing part of their ship time onboard the Ferrel for the recovery of the equipment. Sam Meyers from the CPSD lab is thanked for preparing the equipment for deployment and retrieving the data after recovery. Special thanks to Pam Cox Jutte and the diving team of the SC Department of Natural Resources in helping in the recovery of the tripod. Also, Pam is thanked for her comments and assistance throughout the period of the project. Jane Denny for the US Geological Survey (Woods Hole Branch) is thanked for providing digital bathymetry data of the ODMDS site.

LIST OF REFERENCES

Bishop C.T. and M.A. Donelan, 1987. Measuring Waves with Pressure Transducers. *Coastal Engineering*, 11: 309-328.

Earl, M.D. and J.M. Bishop, 1984. A Practical Guide to Ocean Wave Measurements and Analysis. Endeco, Inc., Marion USA. 78pp.

Foreman, M.G.G., 1977. Manual for Tidal Heights Analysis and Predictions. Pacific Marine Science Report 77-10, Institute of Ocean Sciences, Patricia Bay, Sidney, BC, 97.pp.

Gayes, P.T. 2000. Geophysical characterization of the seafloor within the Charleston Ocean Dredged Material Disposal Site: March-September 2000. Final Report submitted to the South Carolina Department of Natural Resources, Marine Resources Division. 49 pp.

Hill, P., G. Voulgaris and J.H. Trowbridge. 2001. Controls on Floc Size in a Continental Shelf Bottom Boundary Layer. *J. Geophys. Res.*, 106: 9,543-9,549.

Styles, R. and S. M. Glenn, 2000: Modeling stratified wave and current bottom boundary layers on the continental shelf. *J. Geophys. Res*., 101: 24,119-24,139.

Tennekes, H. and J.L. Lumley, 1989. A First Course in Turbulence, MIT Press, 12$^{t,\ 300h}$ Edition, 300pp.

Trowbridge, J. H., 1998. On a technique for measurement of turbulent shear stress in the presence of surface waves. *J. Atmos. Oceanic Technol*. 15: 290-298.

Voulgaris G. and J.H. Trowbridge, 1998. Evaluation of the Acoustic Doppler Velocimeter (ADV) for Turbulence Measurements. *J. Atmos. Oceanic Technol.*, 15(1): 272-289.

Voulgaris, G, J.H. Trowbridge, W.J. Shaw and A.J. Williams, III, 1997. High Resolution Measurements of Turbulent Fluxes and Dissipation Rates in the Benthic Boundary layer. Coastal Dynamics '97: 177-186.

Williams, R., C. Sun and R. Bourgerie, 1997. Collection of Ocean Current Data at the Charleston, South Carolina Ocean Dredged Material Disposal Site. Final Report. National Oceanic and Atmospheric Administration, 14pp plus Figures.

Wilmot, W.H., 1988. Charleston Harbor Oceanography Project Phase 2 Plan. US Department of Commerce, National Oceanic and Atmospheric Administration, National Ocean Service, Office of Oceanography and Marine Assessment.

APPENDICES

APPENDIX I: Results of Harmonic Analysis for Near Bed Currents (approximately 40cm above the Sea Bed at the Charleston ODMDS.

Date: 26-Oct-2001
Number of observations = 1388
Number of good observations = 1387
Record length (in days) = 28.92
Start time: 06-Jul-2001 11:00:00
Raleigh criterion = 1.0
Nodal corrections applied to amplitude and phase relative to center time

Mean Value East Component (x)	= -0.566
Trend	= 0.000
Variance of Raw Time-Series (x)	= 45.2682
Variance of Predicted Time-Series	= 31.8194
Variance of Residuals (xres)	= 13.4488
Percent of Variance Predicted	= 70.3 %

Mean value North Component (y)	= +2.37
Trend	= 0.000
Variance of Raw Time-Series (y)	= 68.4237
Variance of Predicted Time-Series	= 20.6902
Variance of Residuals (yres)	= 47.7335
Percent of Variance Predicted	= 30.2 %

The following Table presents the Tidal Constituents for the nearbed currents, as they were resolved through Harmonic Analysis. The 95% Confidence Intervals of the estimates are also shown.

Tidal Const.	Frequency	Major (cm/s)	95% CI (cm/s)	Minor (cm/s)	95% CI (cm/s)	Inclina-tion(deg)	95% CI (deg)	Phase (degs)	95% CI (deg)	SNR
MSF	0.00282	3.532	1.135	0.109	1.39	72.70	22.64	143.71	18.45	9.7
2Q1	0.03571	0.460	0.714	-0.013	0.68	49.36	82.40	104.55	86.03	0.41
Q1	0.03722	0.692	0.680	-0.338	0.72	140.32	84.31	304.29	81.62	1
O1	0.03873	1.034	0.645	-0.690	0.75	29.31	85.96	125.83	81.21	2.6
NO1	0.04027	0.385	0.687	-0.210	0.71	41.71	165.92	145.71	163.01	0.31
K1	0.04178	0.683	0.776	0.064	0.61	107.67	51.98	332.17	65.58	0.77
J1	0.04329	0.449	0.785	-0.174	0.60	78.18	96.13	206.90	116.85	0.33
OO1	0.04483	0.318	0.789	0.025	0.59	82.80	106.99	192.54	141.51	0.16
UPS1	0.04634	0.405	0.687	-0.193	0.71	138.40	140.21	26.55	137.27	0.35
N2	0.07900	2.583	0.783	-1.588	0.89	173.73	35.90	108.03	33.91	11
M2	0.08051	7.379	0.788	-4.716	0.88	13.46	13.30	290.45	12.67	88
S2	0.08333	1.179	0.869	-0.570	0.80	116.66	57.57	226.38	60.40	1.8
ETA2	0.08507	0.960	0.855	-0.011	0.82	125.54	44.25	129.59	46.15	1.3
MO3	0.11924	0.184	0.204	-0.059	0.15	110.56	57.56	329.78	72.21	0.81
M3	0.12077	0.246	0.184	0.002	0.18	47.62	41.18	90.51	42.57	1.8
MK3	0.12229	0.260	0.145	-0.083	0.21	174.98	52.57	73.06	38.93	3.2
SK3	0.12511	0.184	0.208	-0.081	0.15	76.39	67.56	41.64	84.24	0.78
MN4	0.15951	0.327	0.251	-0.075	0.39	177.73	73.23	126.42	49.07	1.7
M4	0.16102	0.856	0.259	0.170	0.39	168.23	27.16	132.20	18.64	11
MS4	0.16384	0.239	0.394	0.008	0.25	93.11	60.20	305.49	94.29	0.37
S4	0.16667	0.182	0.394	0.125	0.25	94.83	222.80	352.01	258.81	0.21
2MK5	0.20280	0.206	0.260	0.077	0.25	89.09	84.93	352.10	88.00	0.63
2SK5	0.20845	0.130	0.248	-0.085	0.26	10.76	353.69	232.95	228.85	0.27
2MN6	0.24002	0.367	0.182	0.036	0.18	43.50	28.51	349.15	28.41	4.1
M6	0.24153	0.093	0.184	-0.028	0.18	53.06	332.10	126.30	128.22	0.26
2MS6	0.24436	0.075	0.178	-0.048	0.19	23.13	118.00	281.35	276.09	0.18
2SM6	0.24718	0.134	0.178	-0.074	0.19	156.26	214.08	129.35	126.37	0.57
3MK7	0.28331	0.159	0.200	-0.071	0.15	95.79	77.20	302.95	93.36	0.63
M8	0.32205	0.043	0.107	-0.012	0.11	10.68	307.81	154.85	157.46	0.16

Total variance = 113.6919
Predicted variance = 52.5096
Percent of total variance predicted= 46.2 %

APPENDIX II: Results of Harmonic Analysis for Sea Surface Elevation at the Charleston ODMDS.

Number of observations = 1388
Number of good observations = 1387
Record length (in days) = 28.92
Start time: 06-Jul-2001 11:00:00
Raleigh criterion = 1.0
Nodal corrections applied to amplitude and phase relative to center time

Mean Value (x) = 12.01
Trend = 0.000
Variance of Raw Time-Series (x) = 0.30885
Variance of Predicted Time-Series = 0.29667
Variance of Residuals (xres) = 0.012178
Percent of Variance Predicted = 96.1%

Tidal amplitude (n m) and phase (in degs) with 95% CI estimates

tide	freq	amp	amp_err	pha	pha_err	Snr
MSF	0.00282	0.0207	0.040	18.57	110.63	0.27
2Q1	0.03571	0.0008	0.005	43.06	338.35	0.027
Q1	0.03722	0.0260	0.005	134.63	9.96	32
O1	0.03873	0.0687	0.005	139.24	3.81	2.2e+002
NO1	0.04027	0.0104	0.005	176.34	24.59	5.2
K1	0.04178	0.1261	0.005	139.20	2.08	7.5e+002
J1	0.04329	0.0032	0.005	64.35	77.15	0.5
OO1	0.04483	0.0068	0.005	39.87	38.35	2.2
UPS1	0.04634	0.0058	0.005	194.41	44.60	1.6
N2	0.07900	0.1971	0.028	230.80	8.18	49
M2	0.08051	0.7282	0.028	239.32	2.21	6.7e+002
S2	0.08333	0.0937	0.028	274.04	17.26	11
ETA2	0.08507	0.0096	0.028	217.13	151.55	0.12
MO3	0.11924	0.0090	0.003	240.19	17.89	10
M3	0.12077	0.0171	0.003	277.41	9.46	36
MK3	0.12229	0.0045	0.003	318.01	35.88	2.5
SK3	0.12511	0.0051	0.003	214.75	31.78	3.2
MN4	0.15951	0.0063	0.004	281.33	31.64	3.2
M4	0.16102	0.0100	0.004	306.49	19.96	8.1
MS4	0.16384	0.0019	0.004	121.17	103.81	0.3
S4	0.16667	0.0019	0.004	133.93	108.22	0.28
2MK5	0.20280	0.0026	0.003	157.25	69.68	0.66
2SK5	0.20845	0.0082	0.003	285.78	22.31	6.5
2MN6	0.24002	0.0009	0.002	345.08	100.90	0.31
M6	0.24153	0.0020	0.002	69.41	43.94	1.7
2MS6	0.24436	0.0016	0.002	127.94	56.08	1
2SM6	0.24718	0.0006	0.002	120.96	136.86	0.17
3MK7	0.28331	0.0013	0.002	74.38	73.50	0.59
M8	0.32205	0.0006	0.001	355.30	76.43	0.54